

Electronic Supplementary Information

MAPbI₃ microcrystals integrated with Ti₃C₂T_x MXene nanosheets for efficient visible-light photocatalytic H₂ production

Wenbo Li,^{a,b,c} Fang Wang,^{a,b,c} Zhengguo Zhang^{a,b,c} and Shixiong Min^{*a,b,c}

^a *School of Chemistry and Chemical Engineering, North Minzu University, Yinchuan, 750021, P. R. China. E-mail: sxmin@nun.edu.cn.*

^b *Key Laboratory of Chemical Engineering and Technology, State Ethnic Affairs Commission, North Minzu University, Yinchuan, 750021, P. R. China.*

^c *Ningxia Key Laboratory of Solar Chemical Conversion Technology, North Minzu University, Yinchuan 750021, P. R. China.*

**Corresponding author: sxmin@nun.edu.cn*

1. Experimental section

1.1 Chemicals and materials

All chemicals were of analytical grade and used as received without further purification. Methylammonium iodine (MAI, $\geq 99.5\%$) and PbI_2 ($\geq 99.99\%$) were obtained from Xi'an Polymer Light Technology Corp. HI (55~57 wt.% in water) was purchased from Shanghai Titan Scientific Co. Ltd. H_3PO_2 (50 wt.% in water) was received from Shanghai Aladdin Biochemical Technology Co. Ltd. Ti_3AlC_2 powders were purchased from Beijing Dk Nano technology Co., Ltd. LiF was purchased from Aladdin Industrial Corporation. All solutions used throughout the experiments were prepared with ultrapure water (18.2 M Ω cm).

1.2 Preparation of $\text{Ti}_3\text{C}_2\text{T}_x$ nanosheets ($\text{Ti}_3\text{C}_2\text{T}_x$ NSs)

$\text{Ti}_3\text{C}_2\text{T}_x$ NSs were synthesized according to a reported procedure. 2.4 g of LiF was added into 30 mL of 9 M HCl and the solution was allowed to mix thoroughly at room temperature for 10 min. After that, 1.5 g of Ti_3AlC_2 powder was slowly added to above-prepared LiF-HCl aqueous solution to avoid initial overheating due to exothermic nature of the reaction. Then, the temperature was increased to 35 °C and the reaction allowed to proceed under continuous stirring for 24 h. The powder was repeatedly washed with water until almost neutral pH (≥ 6). The freshly produced powder was then dispersed in 100 mL of water and exfoliated with an aid of ultrasonication for 1 h under continuous N_2 bubbling to minimize oxidation. Then, the resulted suspension solution was centrifuged at 3500 rpm for 1 h and the supernatant was collected and freeze-dried to obtain $\text{Ti}_3\text{C}_2\text{T}_x$ NSs powders.

1.3 Preparation of MAPbI₃ and MAPbI₃-saturated HI-H₃PO₂ solution

MAPbI₃ was synthesized by the reaction of MAI (2.56 g) and PbI₂ (7.43 g) in a 25mL of aqueous solution of H₃PO₂ (50 wt %) and HI (57 wt %) at a volume ratio of 1:4. The solution was then heated at 100 °C for 1 h and cooled to room temperature to obtain the saturated solution with MAPbI₃ precipitates. The MAPbI₃ precipitates were separated from the MAPbI₃-saturated solution by centrifugation and dried at 60 °C for 48 h in a vacuum oven to get MAPbI₃ powders, and the obtained MAPbI₃-saturated HI-H₃PO₂ solution was preserved for photocatalytic experiments and photoelectrochemical measurements.

1.4 Preparation of MAPbI₃-Ti₃C₂T_x NS composite photocatalysts

MAPbI₃-Ti₃C₂T_x NS composite photocatalysts were synthesized by a simple in-situ integration method as follows: 100 mg of MAPbI₃ powder and a certain amount of Ti₃C₂T_x NSs (2, 4, 6, 8, 10, or 12 mg) were added to a reaction cell (65 mL) containing 5 mL of MAPbI₃-saturated HI-H₃PO₂ solution. The resulting mixture were ultrasonicated for 5 min. The MAPbI₃-Ti₃C₂T_x NS composite photocatalysts were then either collected by centrifugation for further characterizations or directly used for following photocatalytic H₂ evolution experiment.

1.5 Characterization

X-ray diffraction (XRD) patterns were investigated with a Rigaku Smartlab diffractometer with a nickel filtrated Cu K α radiation. Scanning electron microscopy (SEM) images were taken with a ZEISS EVO 10 scanning electron microscope. Transmission electron microscopy (TEM) and high-resolution TEM (HRTEM) images

were taken with a Tecnai-G²-F30 field emission transmission electron microscope. Atomic force microscopy (AFM) was carried out on a AFMWorkshop TT2-AFM atomic force microscope in tapping mode. X-ray photoelectron spectroscopy (XPS) measurements of the samples were performed on a Thermo Scientific Escalab-250Xi electron spectrometer using an Al Ka X-ray source. Binding energies were referenced to the C 1s peak (set at 284.8 eV) of the sp² hybridized (C=C) carbon from the sample. UV-vis diffuse reflectance spectra were recorded on a PerkinElmer Lambda-750 UV-vis-near-IR spectrometer equipped with an integrating sphere and BaSO₄ powders were used as a reflectance standard. UV-vis absorption spectra were taken with a Thermo Scientific Evolution 220 spectrophotometer. Photoluminescence spectra were determined by a Horiba Scientific FluoroMax-4 spectrofluorometer spectrometer.

1.6 Photocatalytic H₂ evolution experiments

Photocatalytic H₂ evolution experiments were performed with a PCX50C Discover multichannel photocatalytic reaction system (Beijing Perfectlight Technology Co. Ltd.) with white-light LED lamps (10 W×9, 370 nm≤λ≤780 nm) as the light source. Then, the reaction solution was thoroughly degassed by repeated evacuation N₂ filling, and finally refilled with N₂ to reach ambient pressure. After that, the reaction solution was irradiated under continuous stirring. The amount of H₂ produced was manually taken out by a gas-tight syringe (Agilent, 1.0 mL) and analyzed at given time intervals with a precalibrated gas chromatography (Tech comp; GC-7900) with a thermal conductivity detector, a 5 Å molecular sieve column (4 mm×5 m), and with N₂ as carrying gas.

1.7 Determination of solar-to-hydrogen energy conversion efficiency

The solar HI splitting efficiency, so-called solar-to-hydrogen (STH) conversion

efficiency, is the ratio of solar light converted to break the chemical bonding of HI. The standard hydrogen reduction potential is 0 V vs. NHE, and the I⁻ oxidation potential to I₃⁻ is 0.53 V vs. NHE. Because the concentration of I₃⁻ ion in the 5.7 M HI aqueous solution was 1.9 M and the pH of the solution was 0.4, the redox potential could be determined from the Nernst equation as follows:¹

$$E (2\text{H}^+ + 2\text{e}^- \rightarrow \text{H}_2) = 0 - 0.0592 \times 2 \times \log\left(\frac{1}{[\text{H}^+]^2}\right) = 0 - 0.0592 \times \text{pH} = 0.0236 \text{ V vs. RHE}$$

$$E (3\text{I}^- \rightarrow \text{I}_3^- + 2\text{e}^-) = 0.53 + \frac{0.0592}{2} \times \log\left(\frac{[\text{I}_3^-]}{[\text{I}^-]^3}\right) = 0.53 + \frac{0.0592}{2} \times \log\left(\frac{1.9}{5.7^3}\right) = -0.47 \text{ V vs. RHE}$$

For this reason, the total potential for the HI splitting in 5.7 M of HI solution could be calculated as 0.0236 V + 0.47 V = 0.493 V, thus the STH of photocatalytic HI splitting can be calculated as follows:

$$\text{STH (\%)} = \frac{\text{Evolved H}_2 \text{ (mol)} \times 6.02 \times 10^{23} \times 2 \times 0.493 \text{ (eV)} \times 1.6 \times 10^{-19}}{P_{\text{sol}} \text{ (W cm}^{-2}) \times S \text{ (cm}^2) \times t \text{ (s)}} \times 100\%$$

where the P_{sol} (W cm⁻²) is the light irradiation flux, the S (cm²) represents the irradiation area, and the t (s) is irradiation time for H₂ evolution.

According to above equations, in the case of the MAPbI₃ (100 mg)/Ti₃C₂T_x (10 mg), 314.2 μmol of H₂ was evolved after 6 h of light irradiation at 95 mW cm⁻². The light irradiation area was 9.62 cm², the STH was calculated to be 0.15%.

1.8 Electrochemical and photoelectrochemical measurements

The electrochemical and photoelectrochemical measurements were carried out in a standard three-electrode electrochemical set-up using a CS3103 (Wuhan Corrtest Instruments Corp., Ltd) electrochemical workstation. For the fabrication of working electrode, the catalyst suspension was prepared by dispersing 40 mg of catalyst into 5 mL

of toluene solution with a ultrasonication of 30 min. Afterward, the as-prepared catalyst suspension was drop-coated on one side of carbon paper (HESEN, HCP030P, thickness, 0.3 mm) in a glove box. Then, 20 μL of 0.5 wt% Nafion ethanol solution was drop-coated onto the surface of formed catalyst film and the resulted electrode was transferred to a vacuum oven and dried at 60 $^{\circ}\text{C}$ for 6 h. For photocurrent measurements, a saturated Ag/AgCl and a Pt mesh (1 cm \times 1 cm) were used as reference electrode and counter electrode, respectively. A 60 mL of dichloromethane (CH_2Cl_2) solution containing 0.1 M tetrabutylammonium hexafluorophosphate (TBAPF_6) solution was used as the supporting electrolyte. A 300-W white Xe lamp equipped with a cut-off filter of 420 nm was used as the light source. Photocurrent response was recorded by using an amperometric current-time technique at a bias of -0.423 V vs. Ag/AgCl. For electrochemical measurements, a saturated Ag/AgCl and a graphite rod (Diameter: 6 mm) were used as reference electrode and counter electrode, respectively. Potentiostatic electrochemical impedance spectroscopy (EIS) measurements were carried out at a bias of -0.423 V vs. Ag/AgCl with an AC amplitude of 5 mV in the frequency range of 10 mHz to 100 kHz in CH_2Cl_2 solution containing 0.1 M TBAPF_6 as electrolyte. Linear sweep voltammetry (LSV) measurements were carried out in a MAPbI_3 -saturated aqueous $\text{HI}/\text{H}_3\text{PO}_2$ mixed solution at scan rate of 5 mV s^{-1} .

2. Additional figures and tables

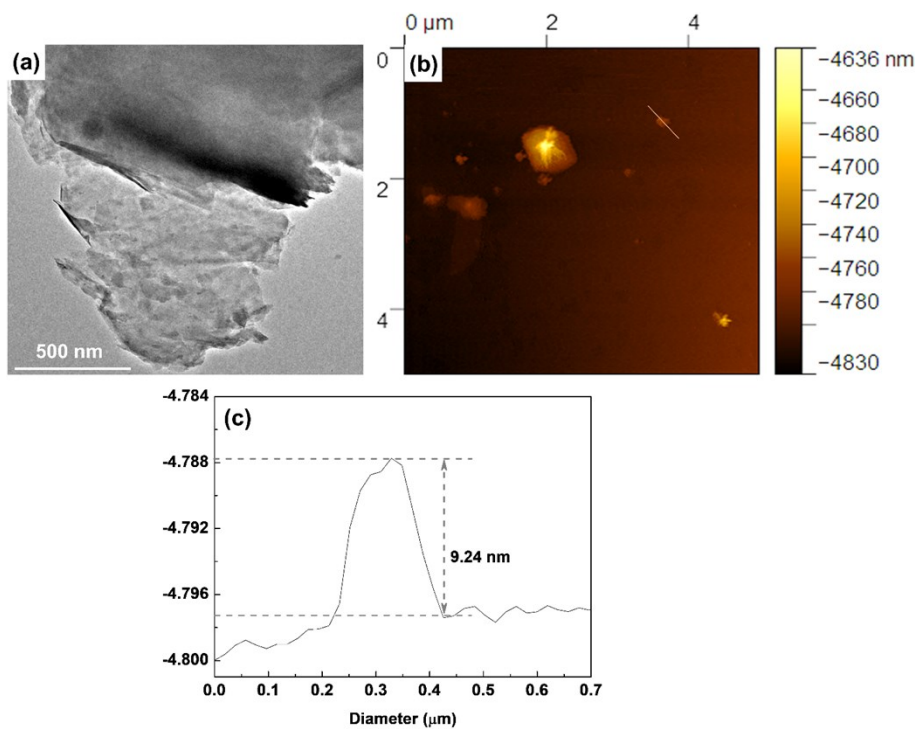


Fig. S1 (a) TEM image of $\text{Ti}_3\text{C}_2\text{T}_x$ NSs. (b) AFM image and (c) the corresponding height profiles of $\text{Ti}_3\text{C}_2\text{T}_x$ NSs.

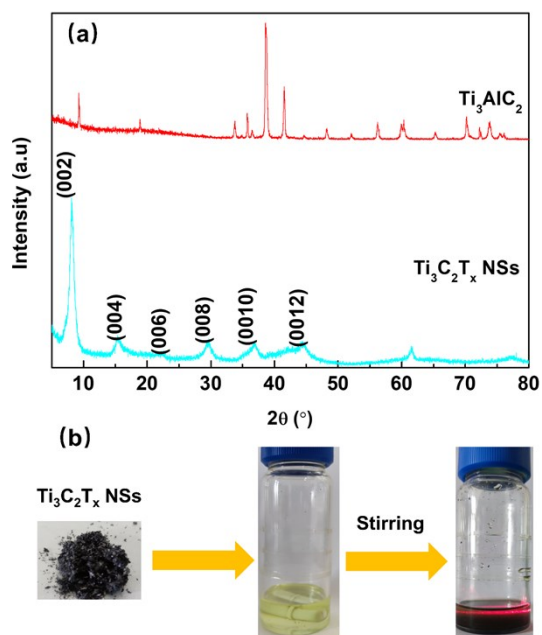


Fig. S2 (a) XRD patterns of Ti_3AlC_2 and $\text{Ti}_3\text{C}_2\text{T}_x$ NSs. The appearance of characteristic

diffraction peaks of the (002), (004), (006), (008), (0010), and (0012) planes in the XRD pattern $\text{Ti}_3\text{C}_2\text{T}_x$ NSs shows the successful transformation of Ti_3AlC_2 MAX into $\text{Ti}_3\text{C}_2\text{T}_x$ MXene nanosheets. (b) The easy dispersion of $\text{Ti}_3\text{C}_2\text{T}_x$ NSs in MAPbI_3 -saturated $\text{HI-H}_3\text{PO}_2$ solution showing an obvious Tyndall effect.

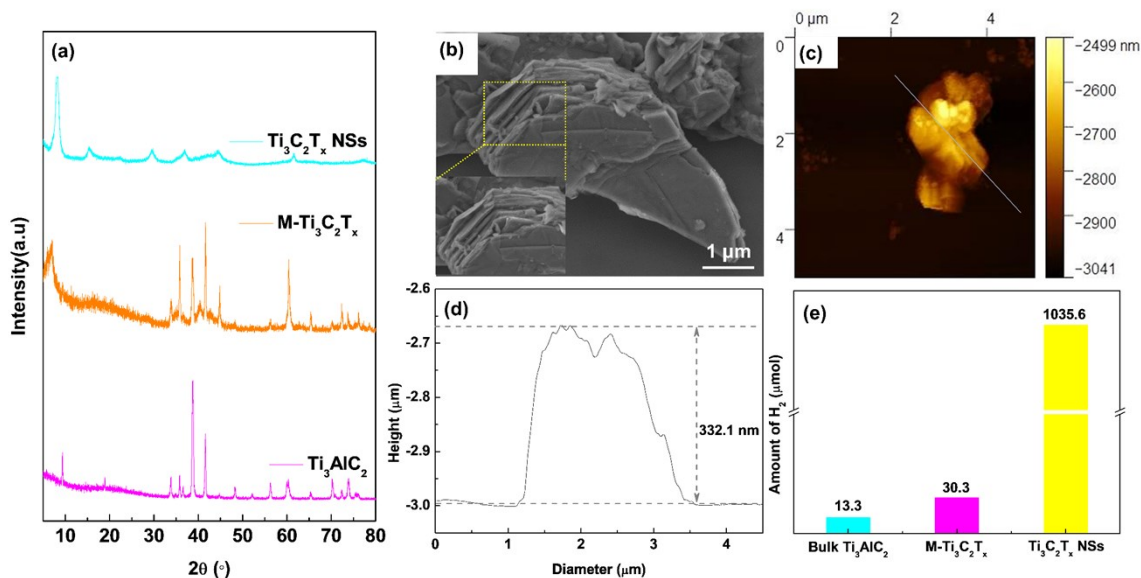


Fig. S3 (a) XRD patterns of $\text{Ti}_3\text{C}_2\text{T}_x$ NSs, M- $\text{Ti}_3\text{C}_2\text{T}_x$, and bulk Ti_3AlC_2 . (b) SEM image of M- $\text{Ti}_3\text{C}_2\text{T}_x$. (c) AFM image and (d) the corresponding height profiles of M- $\text{Ti}_3\text{C}_2\text{T}_x$. (e) Photocatalytic H_2 evolution on the Ti_3AlC_2 (10 mg), MAPbI_3 (100 mg)-M- $\text{Ti}_3\text{C}_2\text{T}_x$ (10 mg), and MAPbI_3 (100 mg)- $\text{Ti}_3\text{C}_2\text{T}_x$ NS (10 mg). Photocatalytic reaction conditions: MAPbI_3 -saturated aqueous $\text{HI-H}_3\text{PO}_2$ mixed solution, 5 mL; Light source, 10-W LED lamp, $370 \leq \lambda \leq 780$ nm; reaction time: 24 h.

In order to clarify the effect of the thickness of the $\text{Ti}_3\text{C}_2\text{T}_x$ on the photocatalytic HER activity, multilayer $\text{Ti}_3\text{C}_2\text{T}_x$ (M- $\text{Ti}_3\text{C}_2\text{T}_x$) was also prepared by etching bulk Ti_3AlC_2 crystals with a LiF/HCl mixed solution without exfoliation and integrated with MAPbI_3 microcrystals for photocatalytic H_2 evolution. The XRD patterns in Fig. S3a show that the Al-layer has been effectively removed from the M- $\text{Ti}_3\text{C}_2\text{T}_x$, but the M- $\text{Ti}_3\text{C}_2\text{T}_x$ is not

fully exfoliated. SEM image of Fig. S3b indicates that the M-Ti₃C₂T_x is layered thick sheet. AFM (Fig. S3c) analysis shows that the thickness of the M-Ti₃C₂T_x is 332.1 nm, which corresponds to *ca.* 339 layers. As a result, the MAPbI₃-M-Ti₃C₂T_x shows much inferior photocatalytic H₂ evolution activity to MAPbI₃-Ti₃C₂T_x NS composite (Fig. S3d). This result clearly indicates that the ultrathin feature of the Ti₃C₂T_x NSs is crucial to enhance the photocatalytic performance of the MAPbI₃ microcrystals. The ultrathin Ti₃C₂T_x NSs cannot only supply large surface area to ensure an intimate contact with MAPbI₃ microcrystals for efficient electron transfer, but also greatly shorten the the electron transfer distance from excited MAPbI₃ to the active sites, all of which but also, all of which are beneficial for suppressing the charge recombination and thus enhancing the activity of photocatalytic H₂ evolution.

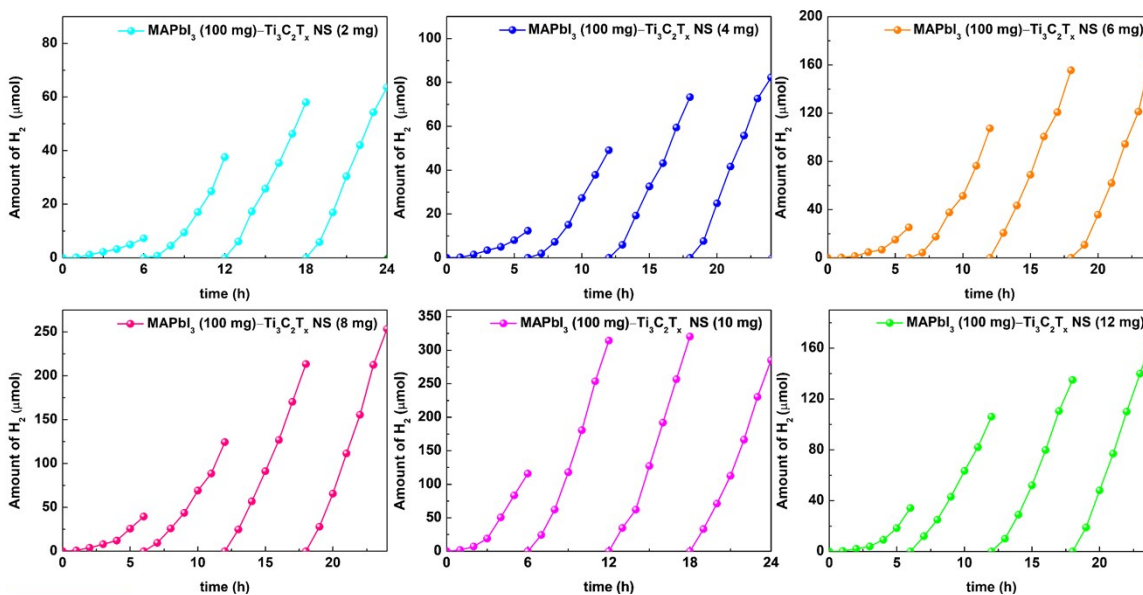


Fig. S4 Time courses of photocatalytic H₂ evolution on MAPbI₃ (100 mg) integrated with different amounts of Ti₃C₂T_x NSs under visible light irradiation. The reaction conditions are kept same as employed for Fig. 1a.

Table S1 Comparison of photocatalytic H₂ evolution of MAPbI₃-Ti₃C₂T_x NS composite with other MAPbI₃-based photocatalysts under visible light.

Catalyst	Reactant solution	Light source	H ₂ evolution activity (μmol h ⁻¹)	Stability	Ref.
MAPbI ₃ -Ti ₃ C ₂ T _x NS	HI solution	10 W LED Lamp (380 nm ≤ λ ≤ 780 nm)	64.61	> 120 h	This work
MAPbI ₃ /MoS ₂ NSs	HI solution	10 W LED Lamp (380 nm ≤ λ ≤ 780 nm)	206.1	> 150 h	2
MAPbI ₃ /Pt/C	HI solution	10 W LED Lamp (380 nm ≤ λ ≤ 780 nm)	68.5	N/A	2
MAPbI ₃ /Pt	HI solution	Solar simulator (λ ≥ 475 nm)	11.4	160 h	3
MAPbI ₃ /rGO	HI solution	300 W Xe lamp (λ ≥ 420 nm)	93.9	200 h	4
MAPbI ₃ /Ni ₃ C	HI solution	300 W Xe lamp (λ ≥ 420 nm)	116.3	200 h	5
MAPbI ₃ /BP	HI solution	300 W Xe lamp (λ ≥ 420 nm)	748.4	200 h	6
MAPbI ₃ /Pt/TiO ₂	HI solution	300 W Xe lamp (λ ≥ 420 nm)	72.8	12 h	7

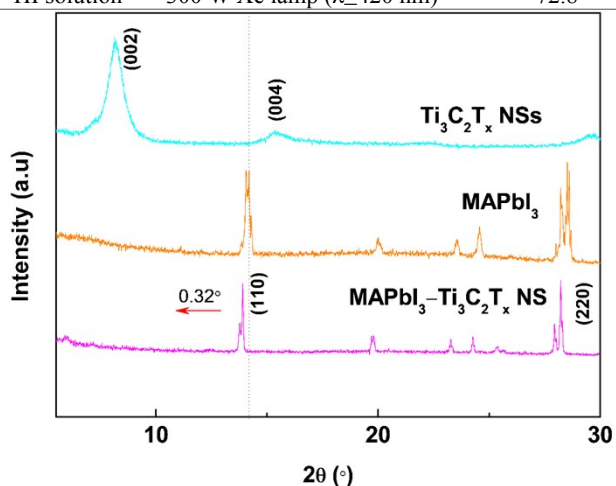


Fig. S5 Enlarged XRD patterns of pristine Ti₃C₂T_x NSs, pristine MAPbI₃, and MAPbI₃-Ti₃C₂T_x NS composite.

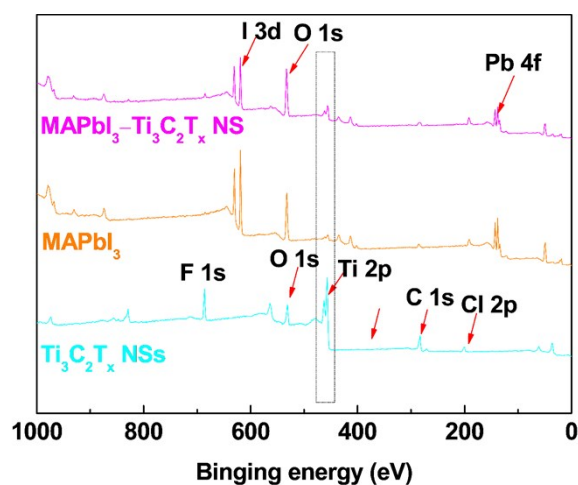


Fig. S6 XPS survey spectra of $\text{Ti}_3\text{C}_2\text{T}_x$ NSs, MAPbI_3 and $\text{MAPbI}_3\text{-Ti}_3\text{C}_2\text{T}_x$ NS composite.

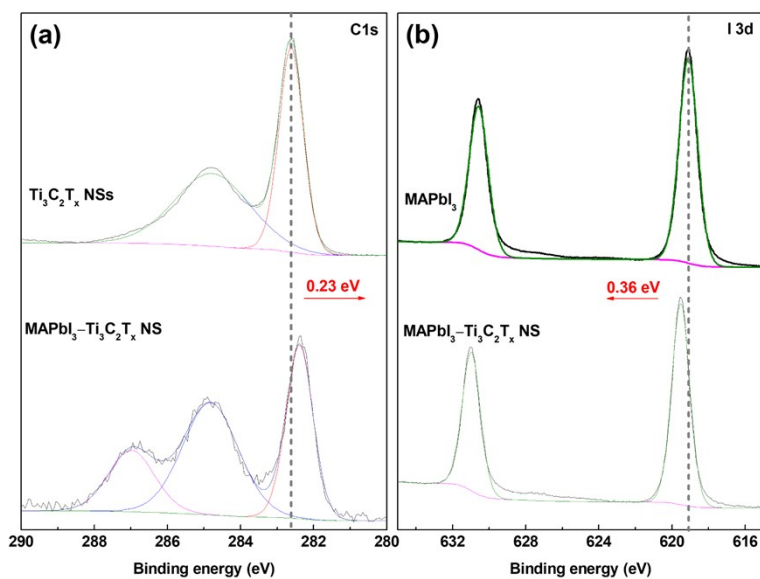


Fig. S7 XPS spectra (a) C 1s of pristine $\text{Ti}_3\text{C}_2\text{T}_x$ NSs and $\text{MAPbI}_3\text{-Ti}_3\text{C}_2\text{T}_x$ NS composite and (b) I 3d of pristine MAPbI_3 and $\text{MAPbI}_3\text{-Ti}_3\text{C}_2\text{T}_x$ NS composite.

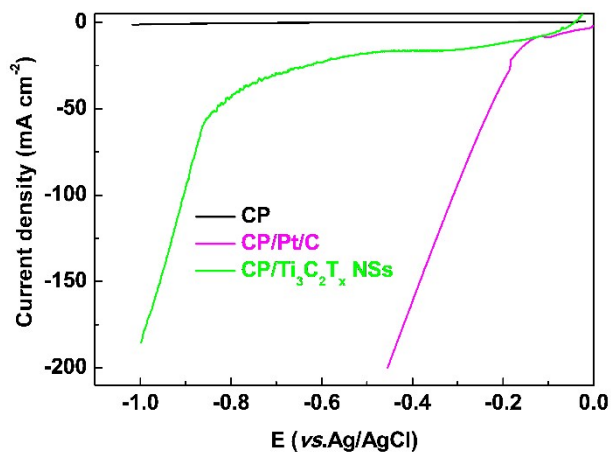


Fig. S8 LSV curves of HER over Pt/C and $\text{Ti}_3\text{C}_2\text{T}_x$ NSs coated on carbon paper (CP) recorded in a MAPbI_3 -saturated aqueous $\text{HI-H}_3\text{PO}_2$ mixed solution at scan rate of 5 mV s^{-1} .

1.

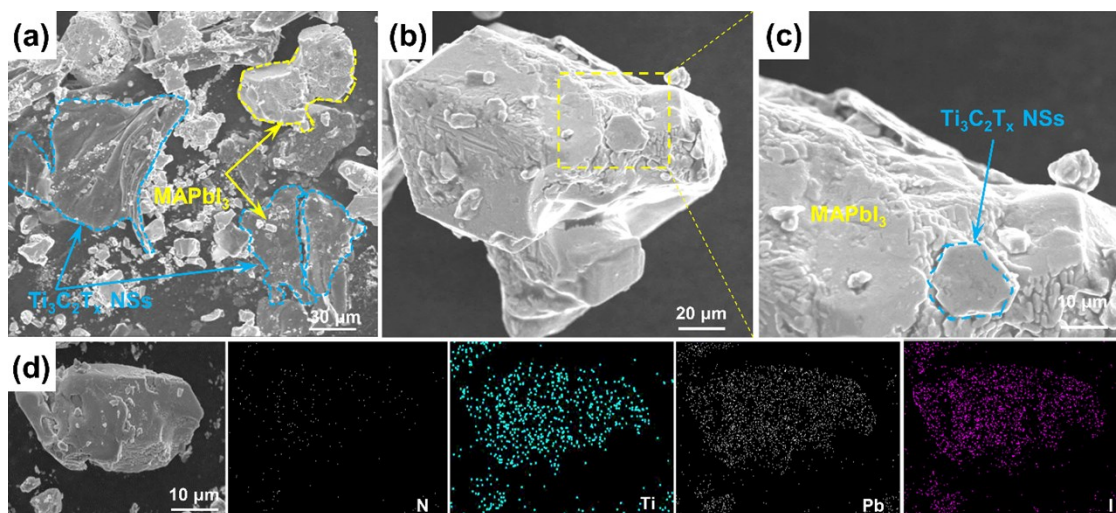


Fig. S9 SEM images of MAPbI₃-Ti₃C₂T_x NS composite after 120 h of photocatalytic H₂ evolution and the corresponding EDS elemental maps of N, Ti, Pb, and I elements.

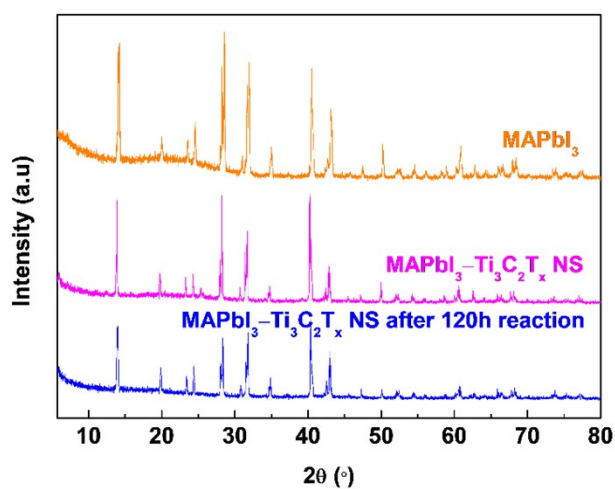


Fig. S10 Comparison of XRD patterns of MAPbI₃-Ti₃C₂T_x NS composite before and after stability test.

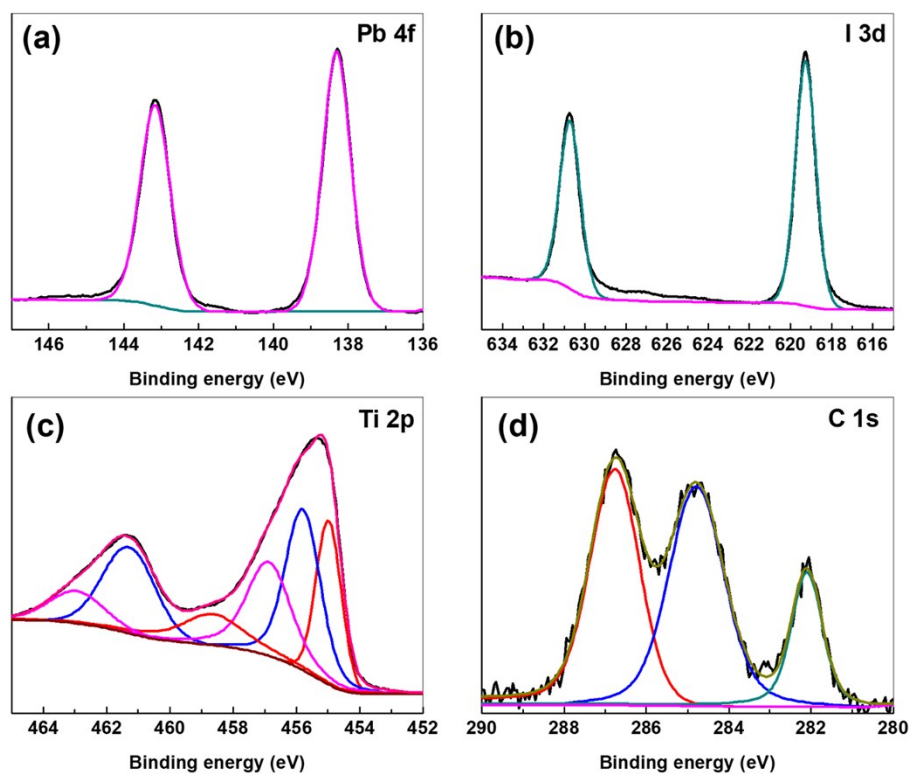


Fig. S11 XPS spectra (a) Pb 4f, (b) I 3d, (c) Ti 2p, and C 1s of MAPbI₃-Ti₃C₂T_x NS composite after stability test.

References

1. H. Wang, H. F. Zhang, J. H. Wang, Y. Y. Gao, F. T. Fan, K. F. Wu, X. Zong and C. Li, *Angew. Chem. Int. Ed.* 2021, **60**, 13.
2. F. Wang, X. Y. Liu, Z. G. Zhang and S. X. Min, *Chem. Commun.*, 2020, **56**, 3281.
3. S. Park, W. J. Chang, C. W. Lee, S. Park, H.-Y. Ahn and K. T. Nam, *Nat. Energy* 2016, **2**, 16185.
4. Y. Wu, P. Wang, X. Zhu, Q. Zhang, Z. Wang, Y. Liu, G. Zou, Y. Dai, M. H. Whangbo and B. Huang, *Adv. Mater.*, 2018, **30**, 1704342.
5. Z. Zhao, J. Wu, Y.-Z. Zheng, N. Li, X. Li and X. Tao, *ACS Catal.*, 2019, **9**, 8144.
6. R. Li, X. Li, J. Wu, X. Lv, Y.-Z. Zheng, Z. Zhao, X. Ding, X. Tao and J.-F. Chen, *Appl. Catal., B*, 2019, **259**, 118075.

7. X. Wang, H. Wang, H. Zhang, W. Yu, X. Wang, Y. Zhao, X. Zong and C. Li, *ACS Energy Lett.*, 2018, **3**, 1159.